# Improved Model of normal-state ARPES line shapes in high temperature superconductors

Rohit Dilip

**Abstract**

We extend the Extremely Correlated Fermi Liquid (ECFL) theory [1] to include a tuning parameter $a$ (which arises in the original ECFL derivation) in the mathematical formalism. The new phenomenologically inspired "aECFL" model improves on the ECFL theory's ability to simultaneously describe energy distribution curves and momentum distribution curves. The aECFL model significantly improves line shape fits in $La_{2-x}Sr_xCuO_4$. The Fermi velocity of the superconducting quasiparticles depends linearly on the $a$ parameter, and the improved fit quality of the spectral function both furthers the ECFL theory and grants valuable insight into the elementary excitations behind the superconducting mechanism in these materials.

**Acknowledgements**

This paper was written for the 2014 Siemens Competition. The research described in this paper was conducted at the Science Internship Program at UCSC over the summer of 2014 under the guidance of Professor Gey-Hong Gweon and Ms. Kazue Matsuyama. They both aided me greatly throughout the course of this project.

## 1 Introduction

The Bardeen-Cooper-Schrieffer (BCS) theory forms the current paradigm in condensed matter physics for describing the phenomenon of superconductivity, which is a material ground state described by precisely zero electrical resistance and expulsion of internal magnetic fields (the Meissner effect). The BCS theory describes the coupling of electrons (known as Cooper pairs) in superconductors due to attractive forces strong enough to overcome the electrons' electrostatic repulsion[1] [2]. The pairing range is generally large compared to inter-electron distances, so Cooper pairs can occupy the same space. Additionally, because each electron has a spin of $\pm\frac{1}{2}$, each Cooper pair acts collectively as a boson. Consequentially, the Pauli Exclusion Principle (which states that two fermions of the same type in a system cannot occupy the same quantum state) does not apply, so Cooper pairs "condense" into the same ground state. The energy gap to break one Cooper pairing then becomes associated with the energy required to break *all* the Cooper pairings, which prevents the normal collisions that generate electrical resistance [2]. Unfortunately, thermal energy above a certain energy gap will break the pairing. Because each individual Cooper pairing is quite weak, the energy gap is quite small and superconductivity only manifests at low temperatures (generally only a few Kelvin), reducing the viability of "traditional" BCS superconductors from an engineering perspective [3].

There is an additional class of known higher temperature superconductors, the most famous of which encompass a number of copper oxide alloys, known as cuprates [4]. The BCS formalism fails to accommodate these superconductors, but their high critical temperatures make them the most viable candidates for technological applications (e.g., 100% efficient energy transmitting wires due to zero electrical resistance, remotely controlled prostheses when employed as ultrasensitive magnetometers, etc.). There is currently no accepted theory that describes these "high temperature superconductors" [4].

[1] In most cases, but not necessarily, this comes from interactions with the crystal lattice of a superconductor.

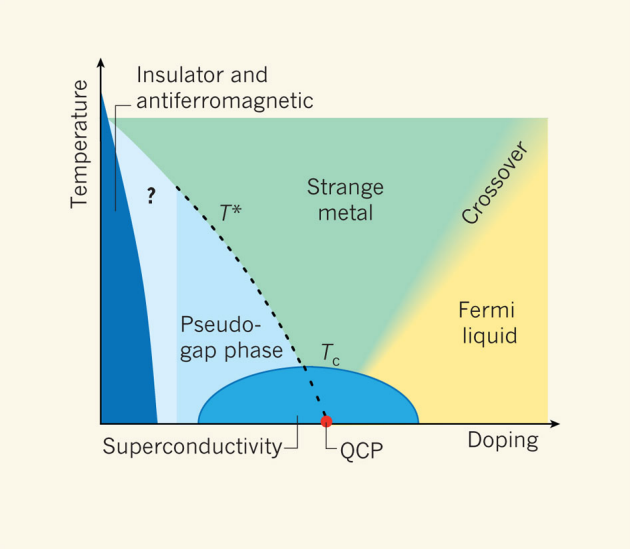


Figure 1: A qualitative phase diagram of a superconductor phase diagram, taken from Varma [5]. The phase diagrams of high temperature superconductors, such as cuprates, are highly complex [4]. Current research suggests that fully understanding the superconducting phase will require further research into the pseudogap and strange metal phases ([5],[6], [7]).

As indicated in Figure 1, the superconducting phase is linked to the pseudogap and strange metal phases [5]. Although the pseudogap is similar to the energy gap, it occurs at temperatures well above the quantum critical temperature. The strange metal phase, also known as the bad metal phase, is characterized by poor conductivity [6]. While this by itself is unremarkable, the reason behind this poor conductivity is not fully understood, since "conventional" physics dictates that these materials should behave like metals and conduct well–hence the name, "strange metals." Moreover, the strange metal phase cannot be easily explained by Landau quasiparticles [4]. Current research suggests that further characterizing the strange metal and pseudogap phases will lead to an increased understanding of the superconducting phase ([6], [8], [9]) and the reasons behind the comparatively high critical temperatures of cuprates.

Describing the states of strongly correlated materials, however, is quite difficult due to the large electron interactions [10]. For weak interactions, Landau's Fermi liquid theory acts as an effective method to model a system of particles [11]. Fermi liquid theory, which can be derived from the microscopic BCS theory [12], characterizes a highly correlated system as one composed of weakly interacting quasiparticles. Each quasiparticle is composed of a particle "dressed" by

the medium through which it propagates [13]. Quasiparticles are considered "elementary excitations" in a material. With high temperature superconductors and other low dimensional materials (so named because a spatial dimension is sufficiently small to restrict the wavefunction of the electrons), however, Landau Fermi liquid theory by itself cannot explain experimental results ([10], [11]).

How does one characterize these materials? A description of the Green's function, a mathematical expression thought to contain significant information about the nature of elementary excitations in materials [14], would provide valuable insight into the different phases of superconductors. The Green's function is linked to the spectral function, which is in turn connected to photoelectron counts from angle resolved photoemission spectroscopy experiments (See Section 3.2). The connection between experimental results and the Green's function provides a method to phenomenologically, if not theoretically, characterize materials. For an experimental cut along a set of $\vec{k}$ values, the relation between photoelectron counts and quasiparticle momentum and energy $I(\vec{k},\omega)$ is a two-dimensional function [14]. The relationship between $I(\vec{k},\omega)$ and the spectral function, $A(\vec{k},\omega)$ is given by Equation 1. For the normal state, the connection between the spectral function and Green's function of a material is expressed in Equation 2.

$$I(\vec{k},\omega) = |M_{if}| f(\omega) A(\vec{k},\omega) \tag{1}$$

$$I(\vec{k},\omega) = \frac{1}{\pi} \Im \left( G(\vec{k},\omega) \right) \tag{2}$$

where $f(\omega)$ represents the Fermi-Dirac distribution, and $M_{if}$ is the dipole matrix element. Current analysis of spectral functions generally uses $I(\vec{k},\omega = \omega_0)$ and $I(\vec{k} = \vec{k}_0,\omega)$, known as momentum distribution curves (MDC) and energy distribution curves (EDC) respectively. This was necessary due to the dichotomy between the two functions. Specifically, in high temperature superconductors, there is a fundamental difference between a momentum distribution curve and applying the dispersion relation to an energy distribution curve [15]. Extracting the spectral function from data has traditionally been very difficult [15], and though some attempts have been made to do so

([7]), [16]), there is no currently accepted theory to describe $I(\vec{k}, \omega)$.

The Extremely Correlated Fermi Liquid (ECFL) state of matter, recently proposed by Shastry [1], was remarkably successful in characterizing the Green's function and spectral function of various materials in the normal state. Although the complete model for low dimensions is very complex, within the limit of high dimensions, the mathematical formalism simplifies dramatically, leaving the simplified ECFL model, also known as the sECFL model ([1], [17]). The sECFL model is well supported experimentally by both conventional and laser ARPES techniques ([18], [19]) (See Section 3.2). The unique properties of this model stem from further "dressing" the quasiparticles (generated from applying Fermi Liquid theory) to account for the extreme correlations ([1], [19]). This is possible because of the "caparison factor" in the ECFL model. Ignoring the remainder of the mathematical formalism, the caparison factor in the sECFL model is shown below.

$$C_n = Q_n \left( 1 - \frac{\omega - \epsilon(\vec{k})}{\gamma_n} \right) \tag{3}$$

where $Q_n$ is the spectral weight per $\vec{k}$ in the $t$-$J$ model, $\omega$ and $\vec{k}$ are the energy and momenta of the quasiparticle, $\epsilon(\vec{k})$ is the dispersion relation between the energy and momentum of the quasiparticle, and $\gamma_n$ relates to the rest of the sECFL formalism. Moreover, the ECFL theory successfully describes experimental results, such as the high energy "kink" examined in Yoshida et al. ([19], [20]). The sECFL model was later expanded into the phenomenological ECFL model by Matsuyama et al. [14], so named because the advancement was inspired by the relative symmetry of the data. The primary change between the sECFL and phenomenological ECFL model was treating the $\omega$ and $\vec{k}$ dependence of $C_n$ as separately adjustable [14]. More specifically, the $\epsilon(\vec{k})$ term is dropped. In the phenomenological ECFL model, if the caparison factor is momentum independent, the model is denoted as the MI-pECFL model. The MI-pECFL model dramatically improved MDC fits, without additional parameters [14]. EDC fits also improve, particularly at cuts far from the Fermi surface. Moreover, the MI-pECFL model, unlike the sECFL model, succeeds in explaining an anomalous feature in ARPES data [9].

In this paper, we present an improved model for describing extremely correlated Fermi liquids, known as the aECFL model. Rather than removing the $\epsilon(\vec{k})$ term altogether from the caparison factor, as was done in the MI-pECFL model, we introduce an extra fit parameter $a$ such that $0 < a < 1$. For $\lim_{a\to 0}$, the aECFL model is simply the MI-pECFL model–similarly, for $\lim_{a\to 1}$, the aECFL model becomes the sECFL model. For all other $a$, however, the effect of the $\epsilon(\vec{k})$ term is lessened, but not entirely removed. The $a$ parameter arises in the derivation of the ECFL theory; the physical significance is discussed later in this paper. To determine whether introducing the $a$ term improved characterization of $I(\vec{k}, \omega)$, we analyzed $I(\vec{k})$ and $I(\omega)$ separately for fixed values of $\omega$ and $\vec{k}$. Because $a$ can take on any value between 0 and 1, there are many possible precise mathematical formalisms, so we developed a technique using $\chi^2$ values per point to equally consider both EDCs and MDCs in analyzing fit quality. Our work has improved the current characterization of the spectral function of high temperature superconductors and has contributed towards the overall success of the ECFL theory.

## 2 Method

The photoelectron counts described by the aECFL model can be primarily characterized through the parameter $a$, which was adjusted for each material to determine whether any particular value of $a$ provided better overall fit results than previous models. We begin by providing some background information, then describe the techniques employed to determine the best overall model.

### 2.1 Acquisition and Rationale of Data

Because this model was proposed to improve upon the pECFL model, we examined the same materials in Matsuyama et al. for ease of comparison. These materials were bismuth strontium calcium copper oxide (Bi-2212) and lanthanum strontium copper oxide (LSCO), both of which are copper oxide (or cuprate) superconductors. This data was acquired at the Stanford Synchrotron Radiation Lightsource at the Stanford Linear Accelerator.

## 2.2 Angle Resolved Photoemission Spectroscopy

Our data is collected via angle resolved photoemission spectroscopy, a very powerful technique where high energy light (ultraviolet or X-ray) is shined on a sample to probe the internal crystal samples [21]. The crystal sample is cleaved to provide a flat surface to irradiate light upon. Due to the photoelectric effect, electrons are excited to higher energy states, and eventually ejected from the sample. Ejected photoelectrons pass through a spectrometer to determine relevant ejection angles and the initial kinetic energies and momenta. Based on these values, a plot of photoelectron count as a function of quasiparticle energy and momentum is created.

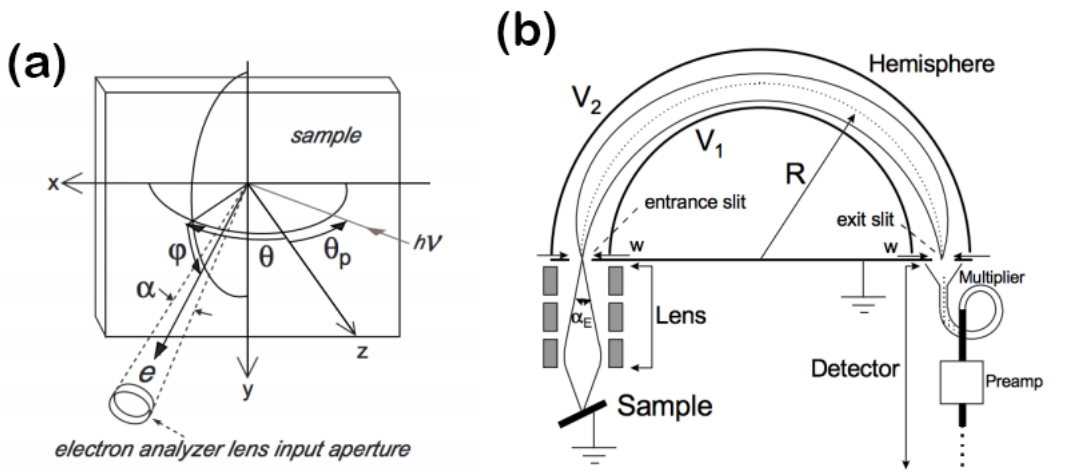


Figure 2: The above figure describes the ARPES experimental procedure. (a) The primary two angles are $\theta$ and $\phi$, which together describe the motion of the photoelectron. While $\alpha$ and $\theta_p$, the angular resolution and the photon incident angle, have significance in finding the angular and energy resolution of the instrument, for the purposes of our calculations, they are unnecessary. Image was taken from Gweon [22]. (b) The ejected photoelectrons pass through a spectrometer, which determine their kinetic energy. The spectrometer is composed of two hemispheres, each charged to a different potential. Incoming photoelectrons will pass through the entrance slit, but will only pass through the exit slit within a certain energy range (the pass energy) owing to the electric field formed between the hemispheres. We can then extrapolate the momentum and kinetic energy of the quasiparticles in the sample based upon the energy and number of photoelectrons. Image taken from Reichwein [21].

### 2.2.1 Overview of ARPES For Photoelectron Counts

ARPES simply acts as a "counting experiment," where the number of ejected photoelectrons is the "intensity." The photoelectron counts can then be used to extrapolate the spectral and Green's functions. Our data is represented in Figure 3.

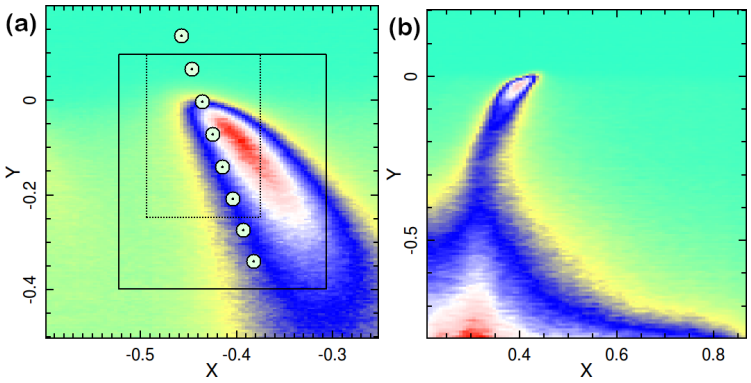


Figure 3: The photoelectron count data for (a) Bi-2212 and (b) LSCO. Momentum is plotted on the x-axis and energy on the y-axis. The intensity–that is, the photoelectron count–is mapped via a color scheme, where red represents the points of highest intensity.

### 2.3 Momentum and Energy Distribution Curves

Our analysis primarily centers around momentum and energy distribution curves (MDCs and EDCs, respectively), which are two dimensional cuts along the three-dimensional photoelectron count function ($I(\vec{k},\omega)$) surface. $I(\vec{k})$ at a fixed $\omega$ represents a momentum distribution curve, while $I(\omega)$ at a fixed $\vec{k}$ represents an energy distribution curve. Historically, high temperature superconductors have displayed a deep dichotomy between MDCs and EDCs ([11], [14], [15]). The main advantage of the initial sECFL model was its ability to simultaneously characterize MDCs and EDCs, as opposed to each separately. Although our ultimate goal is to maintain this duality in our model, we began by fitting the EDCs and MDCs separately for values of $a$ between 0 and 1 in intervals of 0.05[2].

[2]These fits were performed using the GDS Datashop Program (not in the public domain).

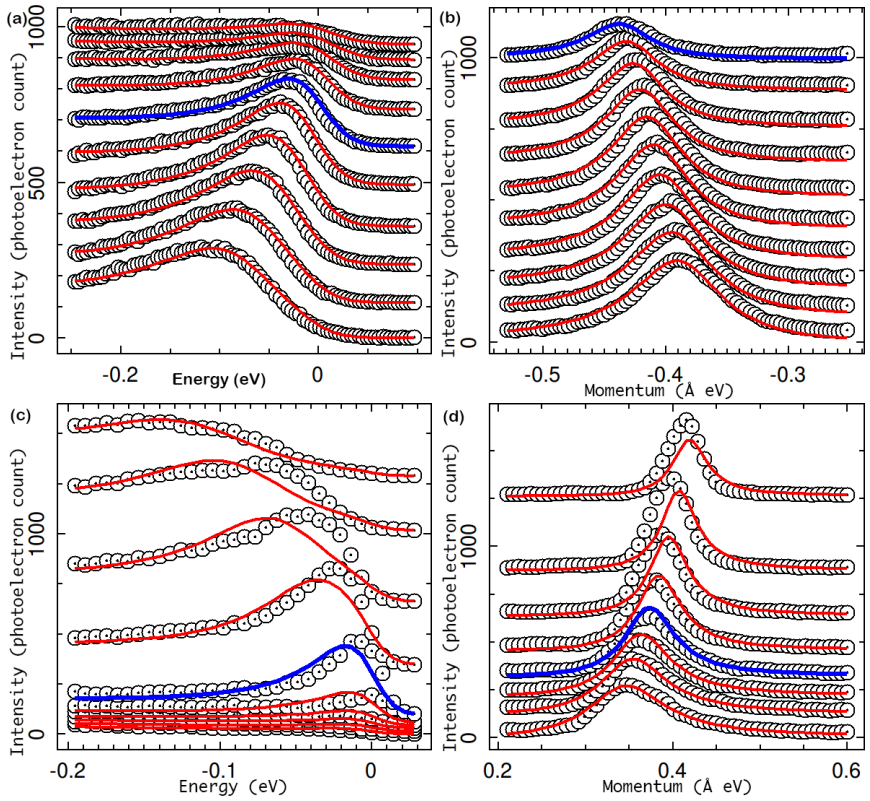


Figure 4: Line shape fits for (a, b) Bi-2212 and (c, d) LSCO energy distribution curves and momentum distribution curves. While the Bi-2212 line shapes are fairly Lorentzian and symmetric, the LSCO line shapes are quite asymmetric. This asymmetry is best modeled by introducing the $a$ term. Furthermore, the line shapes do provide some indication of fit quality, though more specific comparisons (as necessary with small differences in $a$) necessitate a $\chi^2$ comparison. Fits near the blue lines in each plot are most significant. In the EDCs, this is at the Fermi momentum, and in the MDCs, the blue line is at the Fermi energy for Bi-2212 and at high energy for LSCO. Although line shapes near the Fermi energy are significant for Bi-2212, for LSCO, the most significant line shapes are those at energies higher than that in the blue line ($\approx 0.08$ eV). The reasons for this are presented later in this paper.

### 2.4 $\chi^2$ Analysis

As we are primarily concerned with the fit quality to the ARPES data, $\chi^2$ statistical methods are by far the simplest technique to use. However, while we can quite simply generate a $\chi^2$ per point plot of our data, thus easily comparing a relatively small number of $a$ values, such a comparison is not viable to compare a large number of $a$ values. Furthermore, a simple per point comparison cannot determine whether a particular model is overall the best for **both** EDCs and MDCs. As the truly remarkable characteristic of the sECFL and pECFL models is their ability to simultaneously analyze energy and momentum distribution curves, such a comparison is highly desirable [1].

To achieve this, we developed a method to analyze the quality of many such $a$ values. After plotting a $\chi^2$ per point plot, we averaged the $\chi^2$ values across relevant ranges–near the Fermi surface/Fermi momentum for the momentum curves and at the Fermi energy and higher energies for Bi-2212 and LSCO, respectively. Naturally, this was done separately for energy and momentum distribution curves. We then plotted the average $\chi^2$ value as a function of $a$, creating two graphs–one corresponding to EDCs and one to MDCs. This was done for both Bi-2212 and LSCO.

Why high energies for LSCO? Our model is a high temperature model, but while the Bi-2212 experiment was conducted at high temperature (180 K), the LSCO data was collected at low temperature (20 K). For Bi-2212, the full width half maximum values for data at varying temperatures become indistinguishable for $\omega \gtrsim 0.08$ eV [11], suggesting that at higher energies, ARPES line shape temperature dependence is minimized. We can thus use the available low temperature LSCO data if we primarily examine high energies. In doing so, we assume that LSCO and Bi-2212 will behave similarly [14] (not unreasonable, as both are high temperature cuprate superconductors). For the sake of generally comparing the proposed model to previous ones, this approximation is justified. High temperature LSCO data is an attractive avenue of further research, but since our current data is low temperature, we primarily examine high energies.

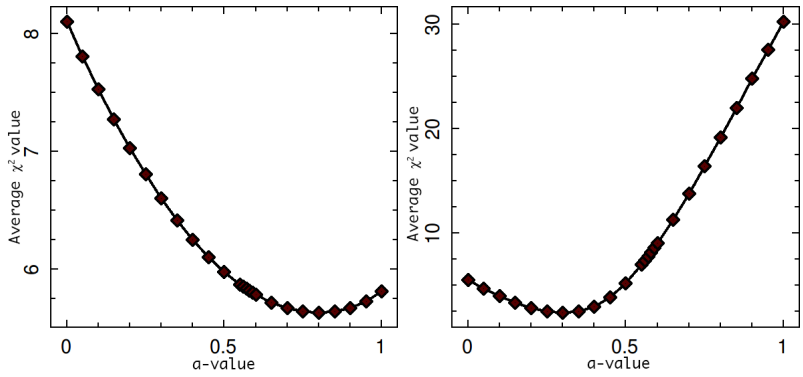


Figure 5: The two plots generated for LSCO, where the left hand and right hand plots are the EDC and MDC $\chi^2$ average versus a plots respectively. By adding these two plots together, we obtain a reasonable idea of which value of $a$ provides the best overall model.

Finally, we equally weighted the importance of the EDC and MDC fit and summed the two plots together. The result tells us which value of $a$ provides the overall best fit.

## 3 Results

### 3.1 aECFL Model Fit Quality

Adding together the two graphs returns the following graph for Bi-2212 and LSCO.

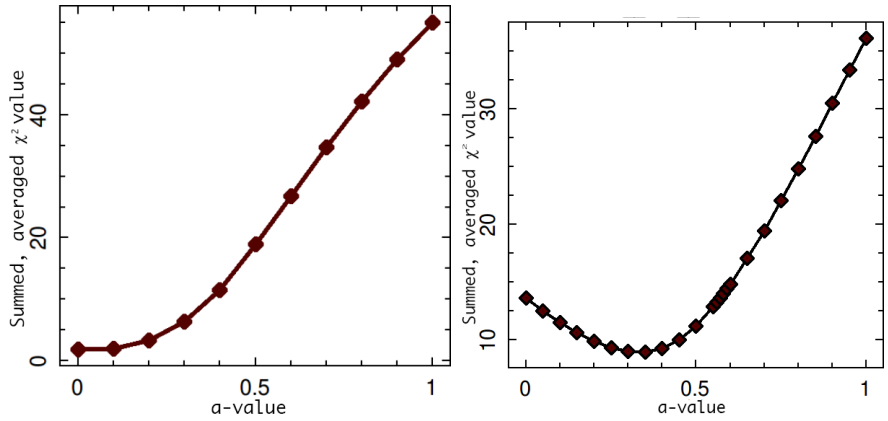


Figure 6: The left hand plot and right hand plot represent the summed, averaged $\chi^2$ value per $a$ value for Bi-2212 and LSCO, respectively. For Bi-2212, the curve is clearly closest to 1 for a=0; however, for LSCO, a=0.35 actually provides the best overall model.

As shown in Figure 6, although a=0, or the MI-pECFL model provides the best quality fit for Bi-2212, a=0.35 provides the best overall fit for LSCO. This observation lends significant credence to the aECFL model. Moreover, since our data points were created in intervals of 0.05, this leads to an error margin of $\pm 0.05$. Thus, we conclude that the best LSCO model occurs at a = 0.35$\pm$ 0.05, which heavily supports the proposed aECFL model.

#### 3.1.1 Changing energy and momenta ranges

Furthermore, the overall best a-value remains consistently at 0.35. In general, the fit quality decreases as the energy or momenta range increases; however, we found that regardless of the range, the overall best model still remained at a=0.35 for LSCO and a=0.00 for Bi-2212.

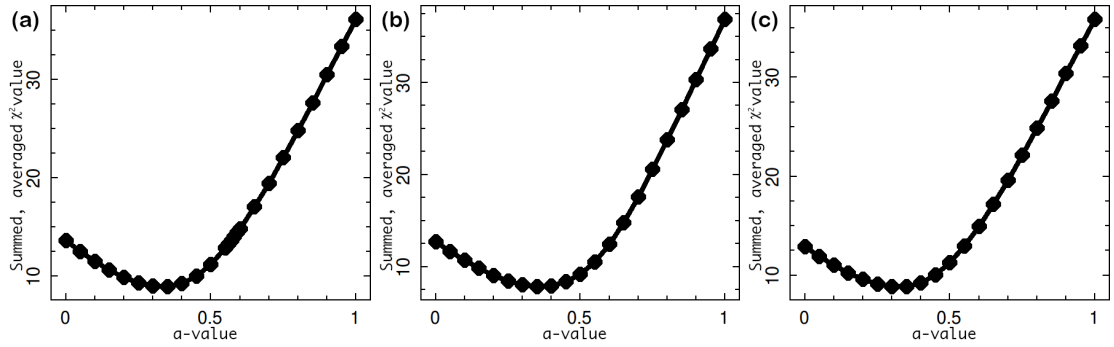


Figure 7: Summed and averaged $\chi^2$ LSCO plots generated as functions of $a$ across a range of (a) 0.35 eV, (b) 0.40 eV, and (c) 0.45 eV. In each case, a=0.35 value clearly provides the best model, inclusive of the a=0 (MI-pECFL) and a=1 (sECFL) models. These findings demonstrate that the best model does not vary between ranges, which would have potentially cast doubt on the reliability of the aECFL model. Similarly, changing the momentum range does not affect the superiority of the a=0.35 model.

The fact that the best model is constant between fittings suggests that the aECFL formalism can consistently provide the best overall model regardless of the energy or momentum ranges over which it is fitted.

### 3.2 Linear interpolation of a-parameter and Fermi velocity

It is known that the single electron dispersion relation can be linearly approximated by

$$\epsilon(\vec{k}) = v_{F0} \times (k - k_F) \tag{4}$$

The quasiparticle group velocity, or Fermi velocity $v_{F0}$, must have some model dependence [14] in order to correctly describe peak positions. For fitting Bi-2212 data, $v_{F0} = 5.5$ for the sECFL model [1] and 6.3 eVÅfor the MI-pECFL model [14]. For fitting LSCO data, $v_{F0} = 4$ for the sECFL model [1] and 5.5 eVÅfor the MI-pECFL model [14]. The only mathematical differentiation between the sECFL and MI-pECFL models is the value of $a$, which implies that the group velocity has some $a$ dependence.

Given that $v_{F0}$ affects the peak position, we found that a first order approximation–a linear

relation between $v_{F0}$ and $a$–provides the best peak position fitting. That is:

$$\textbf{For Bi-2212: } v_{F0} = 6.3 - 0.8 \times a \tag{5}$$

$$\textbf{For LSCO: } v_{F0} = 5.5 - 1.5 \times a \tag{6}$$

Using Equations 5 and 6, we now have the single electron dispersion relations as

$$\textbf{For Bi-2212: } \epsilon(\vec{k}) = (6.3 - 0.8 \times a) \times (k - 0.436) \tag{7}$$

$$\textbf{For LSCO: } \epsilon(\vec{k}) = (5.5 - 1.5 \times a) \times (k - 0.422) \tag{8}$$

Where $k_F$, the Fermi momentum, was determined as the peak position in each material's respective momentum distribution curve taken at the Fermi energy. This linear interpolation was soon determined to successfully characterize the peak positions of the ARPES line shapes, which suggests that the a-$v_F$ relationship can indeed be well approximated as linear.

Furthermore, based on Landau Fermi liquid theory [11], the effective mass of the quasiparticles is given by

$$m^* = \frac{k_F}{v_F} \tag{9}$$

Because the $a$ parameter is clearly linked to the Fermi velocity, it is, in turn, linked to the effective mass of the quasiparticles. Thus, the weight of the dispersion relation in the caparison factor tunes the quasiparticle effective mass in the spectral function model.

## 4 Discussion

As is visible in Figure 8, the aECFL model is several times better in EDC fits and a definite improvement in significant sections of the MDC fits. This is a substantial step forward in understanding pseudogap theory and characterizing the spectral functions of different materials. In particular, this model improves our characterization of the quasiparticle excitations inside a given material, which

are fundamental towards properly understanding the superconducting mechanism.

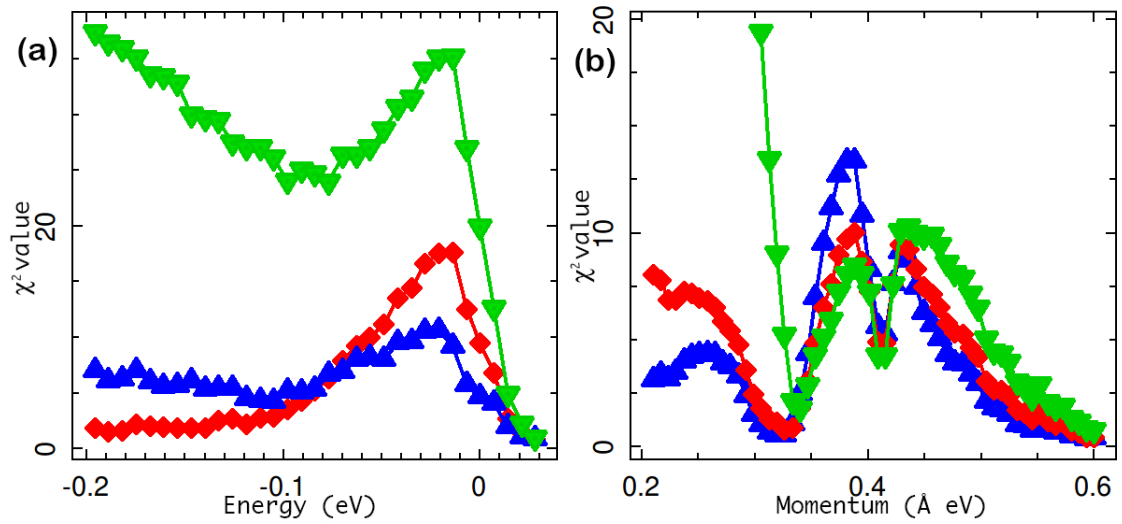


Figure 8: A $\chi^2$ plot for the (a) MDC and (b) EDC line shapes of LSCO, where the red line represents a=0.35, the blue line a=0.00 (MI-pECFL), the green line a=1.00 (sECFL), and the yellow data points represent the ARPES data. Note that because this is a $\chi^2$ plot, the plot corresponding to the energy distribution curve actually has an x-axis of momentum, and vice versa for the momentum-distribution curve (for example, a cut $-\omega = 0.15$ is best represented via the a=0.35 model, as we can see in (a)). We focus on LSCO because it verifies the abilities of the aECFL model, unlike Bi-2212 (while Bi-2212 does indeed have a=0 as the best model, this is merely the MI-pECFL model, and so does not advance the work done by Matsuyama et al. [14].). For higher energies, the red line is definitively the best. Although the MDC $\chi^2$ plot is not quite as evident, near and inside the Fermi surface (all $k < k_F$, the Fermi momentum, given by k=0.422), the red line provides the overall best model. The blue line is clearly worse and the fit corresponding to the green line decreases in quality exponentially farther inside the Fermi surface.

Our results also substantially strengthen the premise of the original sECFL theory [1]. Analyzing photoelectron counts as a whole is a nontrivial task due to the multidimensionality of the count function, and while the original ECFL theory made large steps forward in this regard, it could not describe MDCs very well [1]. The MI-pECFL model was a substantial improvement, particularly for very Lorentzian line shapes [14]. The aECFL model, however, successfully extends both its predecessors to include asymmetric and Lorentzian line shapes. The fact that the aECFL model has been able to further improve characterization of ARPES line shapes seems to indicate the validity of the base ECFL theory.

### 4.1 Reliability of Methods

Ultimately, the goal of this research was to provide the best model for ARPES line shapes, so fit quality is extremely important. Since our research was an extension of previous models, our methods were adapted from those used by Shastry [1] and Matsuyama et al. [14]. Our $\chi^2$ tests initially are unremarkable in of themselves for comparing individual models, as in Figure 8. However, the technique that we developed to simultaneously analyze a large number of $a$ values merits further scrutiny. In this method, we equally weighted the $\chi^2$ averages for EDC and MDC fits. However, the $\chi^2$ average for the MDCs tends to be higher than that for the EDCs, so this weighting system may result in a wider degree of uncertainty as to the absolute best model. Paradoxically, because of the difference in $\chi^2$ values, giving equal importance to both EDCs and MDCs may require that we weight them differently. One potential solution is to compare the ratio of the averages (from a=0.00 to a=1.00) of the $\chi^2$ values as functions of $a$ for the EDCs and MDCs (See Figure 5). However, given that the same weighting was naturally used for every value of $a$, any variation in the concluded "best model" would be slight and within our error margin of 0.05.

Furthermore, we made several assumptions concerning the behavior of LSCO that merit further investigation. As stated earlier in Section 3.4, our LSCO data is taken at low temperatures, which would make it seemingly invalid data for our high temperature model. However, it is well known that at high energy, the full-width half maximum values[3] of the lines shapes of Bi-2212 ARPES data taken at various temperatures converge [11]. This suggests that at high energies, the line shape temperature dependence is minimized. Given the similarities between LSCO and Bi-2212 (both are high temperature, cuprate superconductors), one can assume that LSCO will behave similarly.

### 4.2 Comparison with previous studies

Simultaneously analyzing EDCs and MDCs has long been a desirable, but unachieved, goal. In this paper, we proposed an alternative model to address the shortcomings of both the sECFL model (which by far succeeded the most in uniting the EDC and MDC dichotomy [1]) and the MI-pECFL

[3] The full width half maximum values have significance in our model–they are fundamentally linked to the lifetimes of the quasiparticles in the crystal [23]

model in describing different types of high temperature superconductors. For certain materials, our model definitely provides the best fit as compared to the previous models, as shown in Figure 8.

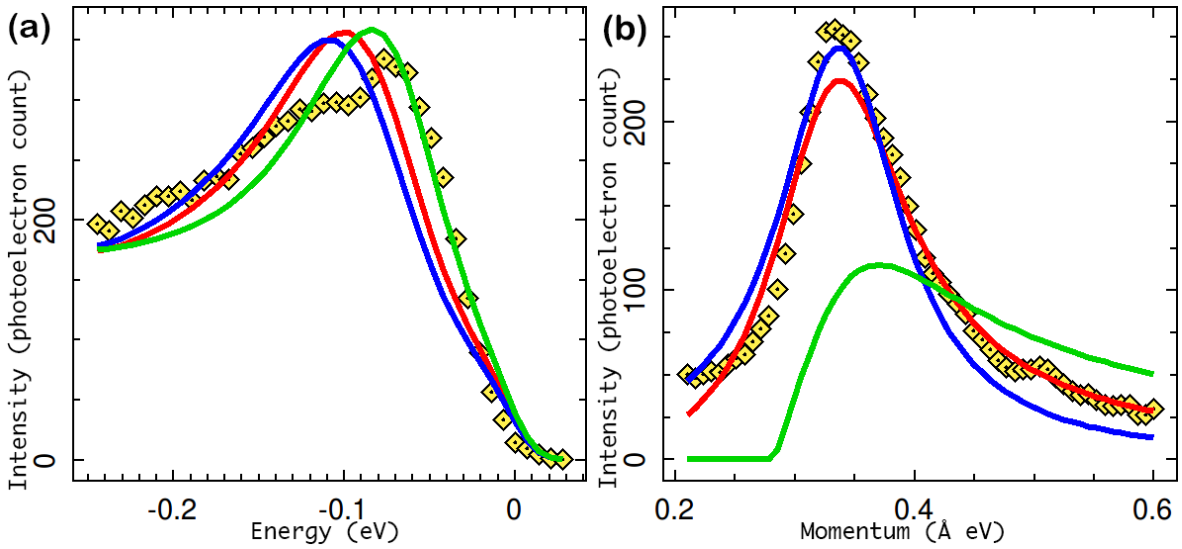


Figure 9: Line shapes of LSCO as EDCs and MDCs, taken with the same color scheme as Figure 8 (red is aECFL (a=0.35), blue is MI-pECFL (a=0), green is sECFL (a=1). The MDC cut is taken at $\omega = 0.19$, and the superiority of the aECFL model is clear. The EDC cut is a little less obvious–it was taken at $k = 0.36$ ÅeV. The aECFL model is clearly superior to the MI-pECFL model. Although the sECFL model is technically better than the aECFL model at this specific point, the fit quality decreases exponentially farther into the Fermi surface (See Figure 8), and the fit does not even succeed across a reasonably momentum range. Thus, we conclude that the aECFL model is indeed superior when compared to the sECFL and MI-pECFL models.

## 5 Conclusions and Future Work

This paper proposed an extension to the sECFL theory [1] to further simultaneously describe energy and momentum distribution curves with a reasonable degree of accuracy. By using the same data as was used in the predecessor MI-pECFL model [14], we could easily compare our model to its predecessors. By averaging $\chi^2$ values and summing the averages for EDCs and MDCs, we found that for certain superconductors, a value of $a$ in the aECFL model provides better EDC and MDC fit quality than either the sECFL or MI-pECFL models. Moreover, we found that the value of $a$ was material dependent, which suggests a deeper physical significance behind this $a$ value. The quasiparticle Fermi velocity was found as linearly dependent with $a$ (to a reasonable approximation), which will be quite useful in later research. Our research has extended the previous line shape analysis [14] to a level of quality unprecedented in prior studies, and has strengthened

the validity of the Extremely Correlated Fermi Liquid theory.

Our work opens up several possible avenues of further research. To further corroborate the aECFL model, high temperature LSCO data would be quite useful. As a matter of fact, this particular avenue of research is quite attractive because it serves a dual purpose. Firstly, we can discover whether the assumption of high energy-low temperature and high energy-high temperature model equivalence, as described in Kaminski et al. [11] is correct. Moreover, finding the $a$ value for high temperature LSCO data that returns the best model would be an effective way to confirm our findings.

Furthermore, in the interest of understanding the mathematical formalism more, it would be highly advantageous to create fits for different materials. Currently, the aECFL model has only been tested on Bi-2212 and LSCO. Different superconductors would help to explain the physical significance of the $a$ parameter in the material's internal mechanisms, as one could compare the physical differences between the materials and their respective $a$ values, and thus identify the defining property between each material that changing $a$ affects. Bi-2212 was ideal because the pseudogap phase is known to be quite strong [20]. Bi-2201 and Bi-2223, two other high temperature superconductors in the Bi-family, would serve as potential materials with which to further test the aECFL model. The different materials are classified based on the number of $CuO_2$ layers in the structure; Bi-2212 is double layered, while Bi-2201 and Bi-2223 are single and triple layered, respectively [24]. Given that ARPES data has already been collected for Bi-2223 in Feng et al. [24], the latter stands out as a particularly attractive option. Additionally, materials such as $Ca_{2-x}Na_xCuO_2Cl_2$, that are cuprates but are not part of the bismuth family, would further help to corroborate the general ECFL theory. $Ca_{2-x}Na_xCuO_2Cl_2$ in particular has a relatively simple structure compared to the Bi-based cuprates or LSCO [25], which would make further ARPES experiments much more viable. Recent research [26] also opens the possibility of using yttrium barium copper oxide (YBCO) as a material with which to test the aECFL model. Although ARPES data was once notoriously difficult to obtain for YBCO, improvements in experimental techniques have led to some progress in this endeavor [26]. Because YBCO has been an area of limited research, due

to the previous difficulties in obtaining useful data, applying the aECFL model now could yield valuable insight into the many-body effects behind the superconducting mechanism.

Generally speaking, it would be beneficial to extend the current model to larger temperature and doping ranges. In this study, we have already extended momenta and energy ranges and found that the model is still consistent, but we have not seen the effect of temperature and doping. As adjusting the doping constant can change the quantum state of matter, it would be beneficial to see how this affects the aECFL model. In the interest of applying our model over a wide variety of situations, applying the aECFL model to laser ARPES techniques (as opposed to conventional ARPES), as was done in Gweon et al. [18] will further strengthen our results.

Additionally, there is another previously introduced model that we have not touched upon in this paper. This is the MD-pECFL model, first proposed by Matsuyama et al. [14] as a way to describe the more asymmetric LSCO MDC fits, while the MI-pECFL model could be used to describe the Lorentzian Bi-2212 fits. The MD-pECFL model was shown to be quite adept at describing the asymmetry in the LSCO fits. Further work includes comparing the aECFL model (for an ideal value of $a$) and the MD-pECFL model, via a simple $\chi^2$ comparison.

Finally, the sECFL model is taken within the limit of high dimensions, as mentioned earlier. Within this limit, terms in the formalism vanish, significantly simplifying our description of the line shapes ([1], [17]). The addition of the $a$ term and our research will hopefully be of some use in the low-dimensional formalism, which is much more complex but very important. It is understood that the $a$ term mathematically arises from the Extremely Correlated Fermi Liquid theory, and the confirmation that it does indeed improve ARPES line shapes furthers the ECFL theory. By further expanding our description of high temperature superconductors, we gain a broader understanding of the different quantum phases and move closer towards fully understanding the superconducting mechanism in these materials.

## References


[1] B. S. Shastry, Physical Review Letters (2011).

[2] J. Bardeen, L. N. Cooper, and J. R. Schrieffer, Physical Review Letters **108**, 1175 (1957).

[3] P. Leboeuf, Physical Review Letters **100**, 1 (2008), arXiv:0704.2310v3.

[4] B. Keimer, S. A. Kivelson, M. R. Norman, S. Uchida, and J. Zaanen, ArXiv e-prints (2014), 1409.4673.

[5] C. Varma, Nature **468**, 184 (2010).

[6] V. J. Emery and S. A. Kivelson, Phys. Rev. Lett. **74**, 3253 (1995).

[7] P. W. Anderson, Phys. Rev. B **78**, 174505 (2008).

[8] J. Kokalj and R. H. Mckenzie, Physical Review Letters **110** (2013), arXiv:1211.1429v2.

[9] G.-H. Gweon, G.-D. Gu, J. Schneeloch, R. D. Zhong, and T. S. Liu, ArXiv e-prints (2013), 1310.4668.

[10] R. W. Hill, C. Proust, L. Taillefer, P. Fournier, and R. L. Greene, **414**, 711 (2001), cond-mat/0112269.

[11] A. Kaminski *et al.*, Physical Review Letters **8**, 1 (2000), 9904390v2.

[12] R. L. Frank, C. Hainzl, R. Seiringer, and J. P. Solovej, ArXiv e-prints (2011), 1102.4001.

[13] R. Mattuck, *A Guide to Feynman Diagrams in the Many-Body Problem*, 2 ed. (Dover Publications, 1992).

[14] K. Matsuyama and G.-H. Gweon, Physical Review Letters , 1 (2012), 1212.0299.

[15] M. R. Norman, M. Eschrig, A. Kaminski, and J. C. Campuzano, Phys. Rev. B **64**, 184508 (2001).

[16] W. Meevasana *et al.*, Phys. Rev. B **77**, 104506 (2008).

[17] B. S. Shastry, Phys. Rev. B **87**, 125124 (2013).

[18] G.-H. Gweon, B. S. Shastry, and G. D. Gu, Physical Review Letters **107** (2011).

[19] D. Hansen and B. S. Shastry, Phys. Rev. B **87**, 245101 (2013).

[20] T. Yoshida, X. J. Zhou, D. H. Lu, and S. Komiya, Journal of Physics: Condensed Matter **19**, 1 (2007), 0610759v1.

[21] E. Reichwein, *A complete analysis of the intrinsic properties of the topological states in $Bi_2Se_3$ by angle resolved photoemission spectroscopy*, Undergraduate thesis, UCSC, 2014.

[22] G.-H. Gweon, *Angle resolved photoemission study of Fermi surfaces and single-particle excitations of quasi-low dimensional materials*, Phd thesis, University of Michigan, 1999.

[23] D. Orgad *et al.*, Physical Review Letters , 2 (2008), 0005457v2.

[24] D. L. Feng *et al.*, Physical Review Letters **88**, 4 (2008), 0108386v1.

[25] K. M. Shen *et al.*, Phys. Rev. Lett. **93**, 267002 (2004).

[26] V. B. Zabolotnyy *et al.*, **76**, 064519 (2007), cond-mat/0608295.